[18F]KS1, a novel ascorbate-based ligand images ROS in tumor models of rodents and nonhuman primates

Naresh Damuka[a], **Nagaraju Bashetti**[b], **Akiva Mintz**[c], **Avinash H. Bansode**[a], **Mack Miller**[a], **Ivan Krizan**[a], **Cristina Furdui**[d], **Bhuvanachandra Bhoopal**[a], **Krishna Kumar Gollapelli**[a], **JV Shanmukha Kumar**[b], **Gagan Deep**[e], **Greg Dugan**[f], **Mark Cline**[f], **Kiran Kumar Solingapuram Sai**[a,*]

[a]Department of Radiology, Wake Forest School of Medicine, Winston-Salem, NC, United States

[b]Department of Chemistry, Koneru Lakshmaiah Education Foundation, Andhra Pradesh, India

[c]Department of Radiology, Columbia University, New York, NY, United States

[d]Department of Internal Medicine, Wake Forest School of Medicine, Winston-Salem, NC, United States

[e]Department of Cancer Biology, Wake Forest School of Medicine, Winston-Salem, NC, United States

[f]Department of Comparative Medicine, Wake Forest School of Medicine, Winston-Salem, NC, United States

Abstract

Over production of reactive oxygen species (ROS) caused by altered redox regulation of signaling pathways is common in many types of cancers. While PET imaging is recognized as the standard tool for cancer imaging, there are no clinically-approved PET radiotracers for ROS-imaging in cancer diagnosis and treatment. An ascorbate-based radio ligand promises to meet this urgent need. Our laboratory recently synthesized [18F] KS1, a fluoroethoxy furanose ring-containing ascorbate derivative, to track ROS in prostate tumor-bearing mice. Here we report cell uptake assays of [18F]KS1 with different ROS-regulating agents, PET imaging in

head and neck squamous cell carcinoma (HNSCC) mice, and doxorubicin-induced rats; PET imaging in healthy and irradiated hepatic tumor-bearing rhesus to demonstrate its translational potential. Our preliminary evaluations demonstrated that KS1 do not generate ROS in tumor cells at tracer-level concentrations and tumor-killing properties at pharmacologic doses. [^{18}F]KS1 uptake was low in HNSCC pretreated with ROS blockers, and high with ROS inducers. Tumors in high ROS-expressing SCC-61 took up significantly more [^{18}F]KS1 than rSCC-61 (low-ROS expressing HNSCC); high uptake in doxorubicin-treated rats compared to saline-treated controls. Rodent biodistribution and PET imaging of [^{18}F]KS1 in healthy rhesus monkeys demonstrated its favorable safety, pharmacokinetic properties with excellent washout profile, within 3.0 h of radiotracer administration. High uptake of [^{18}F]KS1 in liver tumor tissues of the irradiated hepatic tumor-bearing monkey showed target selectivity. Our strong data *in vitro, in vivo*, and *ex* vivo here supports the high translational utility of [^{18}F]KS1 to image ROS.

Keywords

Positron emission tomography imaging; Reactive oxygen species; Ascorbate; Biodistribution, Radioligands; Cancer

1. Introduction

Ascorbate (vitamin C or ascorbic acid) is a furanose-ring containing water-soluble antioxidant [1]. By reducing semistable chromanoxyl radicals, it protects hydrophobic regions of cells, thus generating metabolically active forms of lipid antioxidants [2-4]. Ascorbate is believed to play a dual role in cancer; at lower concentrations [5], it quenches radical species and at higher concentrations [6], it generates reactive oxygen species (ROS). Based on its latter function, it has been used as an adjunct chemotherapeutic agent to ameliorate chemotherapy-induced side effects [6,7] in preclinical and clinical studies of non-small-cell lung cancer (NSCLC), glioblastoma (GBM), head and neck cancer (HNC), colorectal cancer, pancreatic cancer, prostate cancer (PCa) and breast cancer [8]. A lot of research is being carried out on clinical trials to test the efficacy and use of ascorbate in cancer patients [9] as a pro-oxidant at pharmacological doses [10-13]. We propose that a complete understanding of its ROS-based mechanisms at lower doses will significantly advance the tumor-imaging field.

Positron emission tomography (PET) is a noninvasive, fully quantifiable, and highly sensitive imaging modality that can detect biomarkers *in vivo* [14-16]. Researchers are working to develop PET-based radio-tracers to track several forms of short-lived ROS, including superoxide peroxide, hydrogen peroxide, and free radical species [17-25]. Excessive production of ROS can be consequence of many diseases, including cancer, cardiovascular, and neurodegenerative diseases. Quantification of ROS levels in the body by PET imaging could serve as an early cancer diagnosis/screening tool, and add value to prognosis assessment [26,27]. A recent *in vivo* study used [^{11}C]ascorbic acid to define the sodium ion (Na$^+$)-dependent transport mechanisms of ascorbic acid [28,29] and its redox partner dehydroascorbic acid (DHA) in mouse brains and confirmed its oxidative sensitivity [30]. This study highlights ascorbate's *in vivo* intracellular and extracellular

transport system, but the short-lived [11C] PET isotope ($T_{1/2}$ =20 min) might limit its clinical utility.

We designed, synthesized, and screened multiple ascorbate derivatives as a first step towards developing an ascorbate-based, ROS-imaging PET agent for diagnostic applications. We identified KS1, a high-affinity fluoroethoxy derivative of ascorbate as our lead candidate, radiolabeled with [18F], and reported [31] the design, synthesis, radiochemistry, and initial *in vitro* and *in vivo* PET imaging properties of [18F]KS1 in mice with prostate cancer (PCa) [31]. In the project reported here, we used head and neck squamous cell carcinoma (HNSCC) cell lines, SCC-61 and rSCC-61, a genetically matched model of radiation resistance with reported differences in intracellular ROS (SCC-61$_{ROS}$ > rSCC-61$_{ROS}$) [32]. Since, ascorbate interactions depend heavily on concentrations; we evaluated the ROS potency of KS1 at both tracer and pharmacologic concentrations [5] in two different, human-grade tumor cell lines, including SCC-61 and PC3 (human-grade PCa cell line). We report [18F]KS1's (a) cell uptake assays *in vitro* with different ROS-regulating agents, microPET/CT imaging *in vivo* (b) in HNSCC cell lines, and (c) in doxorubicin (ROS inducer)-treated rats. To support the translational potential, we used [18F]KS1 in test-retest PET scans in two healthy rhesus with to demonstrate its safety, reproducibility, and washout properties. Additionally, PET scan was performed in a irradiated hepatic tumor-bearing monkey to study the target selectivity.

2.   Materials and methods

2.1.   Chemicals: DC

DCFDA assay kit (ab113851) and Lipid Peroxidation (MDA) assay Kit (ab118970) were purchased from abcam, USA. OxyIHC Oxidative Stress Detection Kit (S7450), Ascorbate, *tert*-butyl hydrogen peroxide, *N*-acetyl cysteine, catalase, SOD, and doxorubicin hydrochloride were procured from Sigma Aldrich, St. Louis, USA. All the other media samples including pierce bicinchoninic acid protein kit, DMEM/F-12, F-12 K, leibovitz's L-15 media, FBS, and trypsin-EDTA (0.25%) were procured from Thermofisher, USA.

2.2.   KS1 and [18F]KS1 production

KS1 was produced from L-ascorbic acid following our published protection and deprotection steps [31]. [18F]KS1 was produced following our published protocols [31] from the corresponding tosylate in 18(± 1)% decay-corrected radiochemical yield, with a molar activity of ~129.3 ± 5 GBq/μmol, and ~95(± 2)% radiochemical yield, decay corrected to end of synthesis (n = 55 runs).

2.3.   DCFDA ROS measurements

SCC61 and rSCC61 cells (HNSCC) were provided by the Furdui lab (Wake Forest School of Medicine [WFSM]) and grown in DMEM/F-12 (1:1) with 10% FBS. PC3 cells (human prostate cancer cell line) were provided by the Deep lab (WFSM) and grown in F-12 K media with 10% FBS. Cells were cultured at 37 °C containing 5% CO_2. Cellular ROS was measured using a DCFDA assay following the manufacturer's instructions [33]. SCC-61 cells were seeded into 96 black well plates (~25, 000/well) and maintained to attach at 37

°C in 5% CO_2. After overnight incubation, the cells were treated with KS1 (10 μM, 100 μM, and 2 mM). The kit uses *tert*-butyl hydrogen peroxide (TBHP, 110 μM), a common ROS inducer, as a positive control, and *N*-acetyl cysteine (NAC, 0.5 mM), a common ROS suppressor, as a negative control. Cells without any ligand served as the control. All the cells were incubated with KS1 and ascorbate (10 μM/100 μM/2 mM) for 7 h. They were then labeled with DCFDA solution at 25 μM in DMF for 45 min. Fluorescence intensity was measured in a fluorescence spectrophotometer, at the excitation and emission wavelengths of 485 and 530 nm, respectively.

2.4. In vitro cell uptake assays

[18F]KS1 *in vitro* reactivity, binding affinity, and specificity were determined in SCC-61, following previously reported methods [34-36]. After ~1×10^5 cells were seeded into each well of a 6-well culture, the cells were incubated overnight at 37 °C with 5% CO_2 in an incubator. On the day of the assay, fresh solutions of individual ROS blockers (catalase or ascorbate) or inducers (doxorubicin or ferritin) were made at a concentration of 5 μM. An hour later, radiotracer (n = 6 per ROS blocker/inducer, 0.0185 MBq/well) was added, and SCC-61 cells were incubated for 1 h at 37 °C. Uptake assays were initiated by rinsing the cells with 2×2 mL of phosphate buffer at room temperature and terminated after 1 h by rinsing with 1 mL of the ice-cold buffer solution. Residual fluid was removed by pipette, and 200 μL of 0.1% aqueous sodium dodecylsulfate lysis buffer solution was added to each well. The plate was then agitated at room temperature, and 1 mL of the lysate was taken from each well for γ counting [36-38] using a Wallac 1480 Wizard gamma counter (Perkin Elmer, Waltham, MA). In addition, three 20 μL aliquots were taken from each well to determine their protein concentration using a Pierce bicinchoninic acid protein assay kit (Thermo-Fisher, Rockford, IL). Uptake data for each sample from each well and the standard counts for each condition were expressed as counts-per-minute (cpm) of activity and decay-corrected for elapsed time. Cpm values were then normalized to the amount of radioactivity added to each well and its protein concentration and expressed as percent uptake relative to control, %ID/mg of protein in each well (*p 0.05).

2.5. In vivo microPET imaging studies

All animal experiments were carried out with the approval of the Wake Forest School of Medicine Institutional Animal Care and Use Committee. SCC-61 and rSCC-61 cell lines were cultured in DMEM base media and after its removal and washing with DPBS (Lonza), harvested using trypsin-EDTA (Gibco). Cell numbers were calculated using a hemocytometer and the requisite number (1×10^6) suspended in DMEM media, then mixed with growth factor-reduced matrigel (Corning) at a 1:1 ratio and placed on ice. Athymic nude female mice were placed on a heating pad, anesthetized using isoflurane and subcutaneously injected with 1×10^6 cells (in matrigel) subcutaneously near the left shoulder using 28 G insulin syringe. Those bearing subcutaneous SCC-61 and rSCC-61 tumors [39,40] were separated into two groups (n = 5/group, 20 ± 3 g), earmarked for identification, and returned to their cages.

To examine ROS uptake of [18F]KS1, male Wistar rats (n = 4) were injected with doxorubicin (100 mM) intraperitoneally for 7 days, and control rats (n = 4) were injected

with saline. All Mice and rats underwent microPET/CT imaging following the standard 2–3% isoflurane-oxygen anesthesia protocols [36,41-44]. All the rodents were injected *iv* with ~3.7 MBq ± 0.3 (mice) or 10.5 MBq ± 0.2 (rats) of [^{18}F] KS1, and 1 h later, scanned (TriFoil microPET/CT scanner) for 20 min [31]. The images were reconstructed using TriFoil attenuation correction and fourier imaging dicom parameters. Regions of Interests (ROIs) were plotted for tumor and muscle for tumor-bearing mice; heart, liver, kidney, and muscle for the dox-treated and control rats from the fused PET/CT images, and Standard Uptake Values (SUVs) were obtained using PMOD software.

To measure the relative ROS content in the dox- and saline-treated rats, lipid peroxidation assay was performed using MDA peroxidation kit following the established protocols. Briefly, ~10 mg of liver, heart, kidney, and muscle tissues were collected from the rats (post-microPET scans) and homogenized on ice in MDA lysis buffer and centrifuged at 13000xg for 10 min at 4 °C. The protein supernatant (0.2 mL) was mixed with TBA solution (~0.6 mL), followed by incubation at 95 °C for 60 min, and then cooled on ice for further 10 min. After cooling, 0.2 mL of the mixed solution was added to a 96-well microplate and MDA level was measured on microplate reader at 532 nm. Oxidation associated with tissue was calculated with a standard curve following manufacturer's protocol.

2.6. Standard biodistribution studies

Standard biodistribution studies were first performed in normal/healthy ICR mice (n = 8; 4 male, 4 female). Mice were anesthetized with 1% isoflurane-oxygen and administered ~ 3.7–4.6 MBq of [^{18}F]KS1 *via* tail vein injection. They were sacrificed at 5, 30, 90, or 120 min after radiotracer injection, and the organs of interest, including blood, brain, heart, lung, liver, pancreas, spleen, muscle, bone and tail were removed and weighed and radioactivity was counted in a standard dilution of the injectate with a PerkinElmer γ-counter. The same procedure was performed with SCC-61 and rSCC-61 tumor bearing mice after their microPET imaging. All major organs (as stated above plus tumor tissue) were collected and γ-counted. The percentage dose per gram of each dissected tissue (%ID/g) was decay-corrected and calculated. Radioactivity concentration was expressed as %ID/g of radioactivity (*p 0.05). Tumor-to-muscle ratio was calculated.

2.7. Monkey PET/CT imaging

All non-human primates (NHPs) here were provided by the Cline lab. Rhesus monkeys were placed in the GE PET/CT discovery scanner, and a catheter was inserted into an external saphenous vein for tracer injection and fluid maintenance. Body temperature was maintained at 40 °C with a warm-air circulating blanket, and vital signs (heart rate, blood pressure, respiration rate, and temperature) were monitored throughout the scanning procedure [45]. Anesthetized adult male healthy rhesus monkeys (n = 2, 8 years of age, 10 ± 1 kg) received an intravenous dose of [^{18}F]KS1 ~0.33 (± 0.01) GBq. Whole-body scanning (20 min duration) was performed every 30 min after radiotracer injection for 3 h. The same cohort was rescanned with the same radiotracer and imaging parameters 4 weeks after their first scan. The reproducibility of [^{18}F]KS1 was evaluated using the relative difference % between 'test' and 'retest' scans. TRV% (test-retest variability) between both the scan measurements and intra subject standard deviation was evaluated with the coefficient of variance (CV)

% for 'test' and 'retest' measurements. ROIs were drawn manually on the fused PET/CT images across the kidneys, liver, lungs, brain, heart, and muscle using the PMOD software (with NHP atlas) and SUVs were calculated.

In order to test the high ROS target (tumor) selectivity of our radiotracer, we performed PET/CT imaging in an irradiated hepatic tumor-bearing monkey. Following the established protocols of irradiation methods from the Cline lab, a male rhesus monkey (7.1 kg, 12 years of age) received ~8 Gy total body radiation under Institutional Animal Care and Use Committee oversight. [^{18}F]KS1 (0.3 GBq) was intravenously injected and scanned for 20 min after 90 min distribution., following the same protocol as healthy monkeys. ROIs were manually drawn for liver, kidney, and bladder using the PMOD software and SUVs were calculated.

3. Results

3.1. KS1 ROS interactions

We synthesized, and characterized an ascorbate derivative (*E*)– 5-(2-chloroethylidene)– 3-((4-(2-fluoroethoxy)benzyl)oxy)– 4-hydroxyfuran-2(5 H)-one [KS1] (Fig. 1) by starting from *L*-ascorbic acid [46] following our published methods. KS1 yield was at ~23% and was characterized using ^{1}H NMR. To determine whether it changes intracellular ROS concentration, we used a dichlorofluorescin diacetate (DCFDA) intracellular ROS detection assay following the manufacture's protocol [33]. We used two patient-derived tumor cell lines: SCC-61 (HNSCC) and PC3 (PCa) were used. To determine whether at tracer level KS1 generates ROS, we tested it at two concentrations, 10 and 100 μM, for 7 h. Uptake was expressed as mean fluorescent values ± standard deviation (SD) for 6 replicates for each condition (Fig. 2).

Fluorescence at 10 and 100 μM KS1 in SCC-61 was 2718.3 ± 551 and 3139.3 ± 202, respectively while in PC3 it was 3476 ± 892 and 4189 ± 337, respectively. No significant change in the fluorescence was observed between KS1 (10 μM and 100 μM) and controls in both the tumor cell lines. Similarly, ascorbate did not change ROS uptake at either concentrations or in either cell line. Fluorescence was measured hourly for 7.0 h, and no significant changes were observed in fluorescence. We performed the same DCFDA assay with KS1 and ascorbate at pharmacological doses of 2 mM for 7 h in both SCC-61 and PC3 cell lines (Fig. 2). At 2 mM (10,717 ± 492 in SCC-61 and 13,771 ± 300 in PC3), fluorescence intensity increased significantly over that at 100 μM.; it was close to that of positive control, TBHP (*tert*-butyl hydroperoxide). Signal intensity also increased with straight ascorbate but was slightly higher with KS1.

3.2. [^{18}F]KS1 in vitro cell uptake assay in HNSCC cell line

Following our published protocols [31,47-49], we performed *in vitro* cell uptake of [^{18}F]KS1 in the SCC-61 and rSCC-61 cell lines. Several ROS-blocking and -inducing agents [31] were added to the seeded tumor cells 1.0 h prior to adding radiotracer (n = 6 per agent). For each well, gamma (γ) counts-per-minute (cpm) were normalized to the amount of radioactivity added, and the resultant protein concentration was expressed as percent

uptake relative to the injected dose (ID) *i.e.*, % ID/mg. Intracellular [^{18}F]KS1 radioactive uptake in SCC-61 cells at baseline conditions uptake was 63.2(± 3)%, ~35.2(± 2)% less when ROS-blockers, including catalase and ascorbate, respectively were applied. Treatment with the ROS-inducers, doxorubicin (Dox) and ferritin increased radioactive uptake by ~ 44.7(± 3)% and ~70(± 2)% compared to the baseline values (Fig. 3).

3.3. In vivo microPET/CT imaging

To measure the differential ROS uptake of [^{18}F]KS1, microPET/CT imaging experiments were performed in SCC-61 or SCC-61 tumorbearing female mice (n = 5/group, 25 ± 2.5 g). The mice were scanned for 20 min, 1.0 h-post intravenous injection of [^{18}F]KS1 (3.7 MBq ± 0.3). Basic region-of-interest (ROI) analysis of the PET scans (Fig. 4), showed ~35.08 ± 1% greater uptake in the high ROS-expressing SCC-61 tumors than in the rSCC-61 tumors, demonstrating target (tumor) tissue selectivity.

MicroPET imaging was also performed in the dox- and saline-treated rats (n = 4/group). All rats underwent whole-body PET imaging for 20 min, 1.0 h after radiotracer injection (10.5 MBq ± 0.2). The dox-treated rats showed ~53%, ~44%, and ~48% greater uptake of [^{18}F] KS1 in the heart, liver, and kidney, respectively, than did the saline controls (Fig. 5). Lipid peroxidation-based MDA assay (Fig. S1) complemented the high ROS expressions in kidneys and liver, correlating the *in vitro* and *in vivo* measures of radioactive uptake of [^{18}F]KS1.

3.4. Ex vivo biodistribution studies

[^{18}F]KS1 organ biodistribution was determined first in healthy/ normal ICR mice (n = 8; 4 male, 4 female mice, 22 ± 5 g) 5, 30, 90, and 120 min after radiotracer (3.8 MBq ± 0.1) injection (Table 1). [^{18}F]KS1 was cleared from most major peripheral organs from 5 min to 120 min post-injection: specifically blood at 5 min (ID/g = 1.361 ± 0.71) and at 120 min (ID/g = 0.711 ± 0.071); liver at 5 min (ID/g = 9.72 ± 2.55) and at 120 min (ID/g = 2.124 ± 1.12); and kidney at 5 min (ID/g = 14.793 ± 1.33) and at 120 min (ID/g = 4.23 ± 0.77). No significant uptake was seen in the bone, indicating no defluorination of the radiotracer.

We then examined post-PET biodistribution in SCC-61 and rSCC-61 tumor-bearing mice injected with [^{18}F]KS1 (Fig. 6). SCC-61 tumor mice showed 2.5-fold higher target (tumor) to non-target (muscle) ratio (10.93) compared to the rSCC-61 ratio (4.11). Liver and kidneys showed high radioactivity—potential metabolism and excretory sites, seen with some small molecule-based PET radiotracers [27,50,51]. The radioactive profile in other (non-tumor) organs resembled the distribution kinetics in the healthy/normal mice.

3.5. PET/CT imaging in monkeys

Whole-body PET/CT images in two healthy male rhesus and their repeat scans after 4 week), demonstrated high uptake in kidney, bladder, intestine, and liver (Fig. 7). High uptake of these organs are commonly observed with [^{18}F]-based ROS agents and ascorbate-based compounds. There was no significant bone uptake, indicating no deflorination of the radiotracer.

Test and retest scans did not show significant difference in [^{18}F] KS1's molar activity (110.3 ±3.7 GBq/µmol), radiochemical purity (>98%), and injected dose (0.33 ± 0.01 GBq). ROIs were drawn, and SUVs were calculated for heart, lungs, liver, kidneys, brain, and muscle using PMOD software built with NHP atlas. Both test and retest scans demonstrated a high correlation between SUVs (r = 0.78) in all the organs of interest (Fig. S2). Reproducibility was calculated using the relative difference and absolute variability between the test and retest scans. The relative difference of SUV in organs of interest varied from – 0.4 to – 10%, and the absolute variability between the scans of the same ROIs was ~0.6%. Whole-body PET/CT images taken from 30 to 180 min after radiotracer injection demonstrated excellent washout kinetics from all critical organs, including ~94% in kidneys (from 84.3 to 4.5 KBq/cc), ~80% in liver (from 37.7 to 8.7 KBq/cc), ~89% in heart (from 11.3 to 1.3 KBq/cc), and ~87% in lungs (from 16.8 to 2.1 KBq/cc) (Fig. 7C). Both test and retest scans showed very little brain uptake, suggesting the radiotracer may not be ideal for brain imaging. More importantly, the tumor-bearing monkey demonstrated ~8-fold higher tumor to muscle ratio (72.23 Vs. 9.21 KBq/cc) (Fig. 7B). The generation of ROS in radiated tumor monkey showed in the Fig. S3. All vital signs, including heartbeat, temperature, and pulse, remained stable throughout the scan time and 48 h after radiotracer injection, indicating a preliminary [^{18}F]KS1 safety profile.

4. Discussion

We previously demonstrated [^{18}F]KS1's selectivity and specificity for ROS by measuring *in vitro* PC3 cell uptake and performing microPET imaging with it in PC3-bearing mice. Before conducting the in-depth series of ROS-specific assays, including the ESR, EPR, and PEGylation and other auto-oxidation tests are required to establish the complete mechanistic pathways of KS1/ROS interactions (intra- and extracellularly), we had to demonstrate that KS1 does not act as a pro-oxidant to validate [^{18}F]KS1 as potential PET ROS imaging agent at tracer concentrations (0.1 mM). Many believe that at pharmacologic concentrations, ascorbate may act as pro-oxidant [52] in tumor cells [8]. The maximum-allowed concentration for a typical clinical PET radiotracer is < 100 µM [53]. Therefore, we chose 10–100 µM as our concentration range for tracer-level assays. The lowest reported pharmacologic dose for ascorbate is 2.0 mM [54], so we selected 2.0 mM as our high-concentration dose. We performed a DCDFA assay to evaluate KS1 ROS interactions in tumor cells *in vitro*. Ligand incubation times were based on the maximum tracer uptake time (~2 h) for a typical [^{18}F]-based PET radiotracer injection [55]. Fluorescence with KS1 at concentrations of 10 µM and 100 µM did not increase intracellular ROS in either SCC-61 or PC3 cell lines. We performed the same DCFDA assay with KS1 and ascorbate at pharmacological doses (2 mM) for 7 h in both SCC-61 and PC3 cell lines and found that high ROS generation increased fluorescence signal. These results demonstrate that our ligand at 100 µM concentration does not increase intracellular ROS in an intact tissue.

Next, we performed *in vitro* cell uptake studies in HNSCC's SCC-61 and rSCC-61 cell lines using ROS-blocking agents, including catalase and ascorbate, or ROS-inducing agents, including doxorubicin and ferritin at 100 µM. SCC-61 have greater ROS content and protein oxidation than rSCC-61 [56-58], and in our previous publication we reported that [^{18}F]KS1 cell uptake has ~51% greater uptake in SCC-61 than in rSCC-61. ROS blockers (catalase

and ascorbate) reduced the baseline uptake validating [^{18}F]KS1 specificity for ROS *in vitro*. Ferritin, a protein that contributes to iron-storage, stimulates ascorbate production by forming ROS [59,60] and increased radiotracer uptake ~70%. Dox is a highly effective anticancer drug frequently used to treat hematological and solid tumors; it primarily acts by forming superoxide peroxide [18, 32, 61-66]. Treatment with dox increased [^{18}F]KS1 uptake by ~44%. These low increases may be attributed to the *in vitro* nature of ferritin and dox-based assays and the timing/dosages of our incubations [31]. Cellular uptake studies suggest some degree of nonspecific binding commonly associated with radiotracer evaluations of cancer [17-25]. These *in vitro* cell uptake studies with different blockers and inducers serve as a "gain-of-function/proof-of-principle" [36,67] analysis of KS1. They demonstrate superior [^{18}F]KS1 selectivity and specificity in tumor cells with high ROS levels.

After evaluating ROS uptake of [^{18}F]KS1 in an HNSCC cell line *in vitro*, we performed *in vivo* microPET/CT scans in the same tumorbearing mice. From microPET/CT PMOD analyses, uptake in high ROS-expressing SCC-61 tumors was ~35% higher than that in rSCC-61 tumors, demonstrating target (tumor) tissue selectivity.

To further validate the imaging potency of [^{18}F]KS1, we performed PET imaging in a dox-induced ROS rat model. Dox induces cell cytotoxicity in organs such as heart, liver, and kidneys primarily through superoxide anion formations. Muscle was selected as the background tissue and showed minimal or no uptake. PET imaging with [^{18}F]KS1 in dox-treated rats showed ~44–53% increase in heart, liver, and kidney uptake over that in saline-treated controls. To correlate [^{18}F]KS1 *in vivo* uptake, we used standard lipid peroxidation method with the commercially available MDA-kit *ex vivo* to evaluate the ROS levels of the associated tissues. The kit detected slightly higher ROS in the dox-treated kidneys and liver than in saline-treated controls, corroborating our *in vivo* PET measures.

To determine the accumulation and clearance patterns of [^{18}F]KS1, we first evaluated its biodistribution in healthy/normal mice at multiple time-points including, 5, 30, 90, and 120 min after radiotracer injection. High kidney and liver uptake were common at 60 min post-injection. [^{18}F]KS1 biodistribution showed favorable pharmacokinetics, including rapid washout of activity from peripheral organs, renal and/or hepatic clearance, and insignificant bone uptake (no significant defluorination). Its poor brain uptake indicated that [^{18}F]KS1 may not be used to track ROS in brain. Additionally, [^{18}F]KS1's higher tumor uptake in SCC-61 tumor-bearing mice *ex vivo* establishes that it can clearly distinguish high from low ROS tumors. These biodistribution results corroborate the *in vitro* cell uptake and *in vivo* microPET/CT imaging results.

To further evaluate [^{18}F]KS1's translational potential, we performed whole-body scanning (20 min) every 30 min post-radiotracer injection for 3 h in two healthy adult male rhesus monkeys and rescanned them after 4 weeks to confirm reproducibility. The PET biodistribution profile based on SUVs demonstrated excellent washout kinetics from most of the critical organs from 30 to 180 min post-radiotracer injection. Bladder was slightly radioactive, which might be from the nature of metabolism of an ascorbate-based compound.

Rhesus monkeys exposed to radiation experience precipitous drops in their peripheral blood lymphocyte counts, increased target tissue ROS and persistent systemic inflammation for years after exposure, and differential regulation of ascorbic acid regulated pathways. Therefore, forms an ideal animal model to validate our ascorbate-based PET radioligand strategy to image ROS *in vivo*. These models have previously demonstrated high oxidative stress, inflammation, and other pathologic markers [68-70]. Our PET imaging study with the irradiated hepatic tumor monkey demonstrated ~8-fold high radiotracer uptake in the liver tumor tissues compared to the non-tumor muscle tissue (background). While we understand the limitation of an imaging study in one (tumor-bearing) monkey here, our primary purpose was to evaluate [^{18}F]KS1's preliminary imaging potential including feasibility, safety, kinetics, and selectivity.

Taken together, our *in vitro* cell uptake, *in vivo* PET imaging, and *ex vivo* biodistribution findings demonstrated that [^{18}F]KS1 uptake was strong, with high specificity and selectivity, in tumor-bearing mice and monkeys. Its pharmacokinetics, with excellent washout from peripheral organs was favorable. PET imaging data in monkeys support its translational promise of [^{18}F]KS1 for ROS imaging.

5. Conclusions

The DCDFA assays demonstrate that at tracer concentrations, KS1 does not raise ROS levels in tumor cells. *In vitro* cell uptake studies showed greater [^{18}F]KS1 uptake in SCC-61 cells, which express more ROS than rSCC-61 cells, and differential uptake with ROS blockers/ inducers demonstrated its selectivity for ROS. MicroPET/CT imaging and biodistribution data in tumor-bearing mice demonstrate high uptake in the target (tumor) tissue with favorable pharmacokinetics. Moreover, initial PET evaluations of [^{18}F]KS1 in non-human primates exhibited a favorable safety profile, high reproducibility, and pharmacokinetics. Preliminary PET imaging of [^{18}F]KS1 in a hepatic tumor-bearing monkey demonstrated high target selectivity. These strong preliminary data supports the translational promise of [^{18}F]KS1 in tracking ROS *in vivo*. We are conducting blood metabolite, dosimetry studies, and extensive imaging studies in NHP tumor model of radiation to evaluate complete PET imaging properties of [^{18}F]KS1.

Supplementary Material

Refer to Web version on PubMed Central for supplementary material.

Acknowledgments

Data availability

Data will be made available on request.

Abbreviations:

PET	Positron Emission Tomography
ROS	Reactive Oxygen Species
NSCLC	non-small-cell lung cancer
HNC	head and neck cancer
GBM	glioblastoma
PCa	prostate cancer
EOS	end of synthesis
cpm	counts per minute
ROI	regions of interest
SUV	standard uptake value
THBHP	tertiary butyl hydrogen peroxide

References

[1]. Svirbely JL, Szent-Györgyi A, The chemical nature of vitamin C, Biochem J. 27 (1) (1933) 279–285. [PubMed: 16745082]

[2]. Du J, Cullen JJ, Buettner GR, Ascorbic acid: Chemistry, biology and the treatment of cancer, Biochim. Et. Biophys. Acta (BBA) - Rev. Cancer 1826 (2) (2012) 443–457.

[3]. Bhattacharya S, Sarkar R, Nandi S, Porgador A, Jelinek R, Detection of reactive oxygen species by a carbon-dot–ascorbic acid hydrogel, Anal. Chem 89 (1) (2017) 830–836. [PubMed: 27991760]

[4]. Liu S, Ellars CE, Edwards DS, Ascorbic acid: Useful as a buffer agent and radiolytic stabilizer for metalloradiopharmaceuticals, Bioconjugate Chem. 14 (5) (2003) 1052–1056.

[5]. Buettner GR, Jurkiewicz BA, Ascorbate free radical as a marker of oxidative stress: An EPR study, Free Radic. Biol. Med 14 (1) (1993) 49–55. [PubMed: 8384150]

[6]. Putchala MC, Ramani P, Sherlin HJ, Premkumar P, Natesan A, Ascorbic acid and its pro-oxidant activity as a therapy for tumours of oral cavity – A systematic review, Arch. Oral. Biol 58 (6) (2013) 563–574. [PubMed: 23477602]

[7]. Creagan ET, Moertel CG, O'Fallon JR, Schutt AJ, O'Connell MJ, Rubin J, Frytak S, Failure of high-dose vitamin C (ascorbic acid) therapy to benefit patients with advanced cancer, N. Engl. J. Med 301 (13) (1979) 687–690. [PubMed: 384241]

[8]. Nauman G, Gray JC, Parkinson R, Levine M, Paller CJ, Systematic review of intravenous ascorbate in cancer clinical trials, Antioxid. (Basel) 7 (7) (2018) 89.

[9]. Hoffer LJ, Levine M, Assouline S, Melnychuk D, Padayatty SJ, Rosadiuk K, Rousseau C, Robitaille L, Miller JWH, Phase I clinical trial of i.v. ascorbic acid in advanced malignancy, Ann. Oncol 19 (11) (2008) 1969–1974. [PubMed: 18544557]

[10]. Karlowski TR, Chalmers TC, Frenkel LD, Kapikian AZ, Lewis TL, Lynch JM, Ascorbic acid for the common cold: A prophylactic and therapeutic trial, JAMA 231 (10) (1975) 1038–1042. [PubMed: 163386]

[11]. Cameron E, Campbell A, The orthomolecular treatment of cancer II. Clinical trial of high-dose ascorbic acid supplements in advanced human cancer, Chem. Biol. Inter 9 (4) (1974) 285–315.

[12]. ter Riet G, Kessels AGH, Knipschild PG, Randomized clinical trial of ascorbic acid in the treatment of pressure ulcers, J. Clin. Epidemiol 48 (12) (1995) 1453–1460. [PubMed: 8543959]

[13]. Stephenson CM, Levin RD, Spector T, Lis CG, Phase I clinical trial to evaluate the safety, tolerability, and pharmacokinetics of high-dose intravenous ascorbic acid in patients with advanced cancer, Cancer Chemother. Pharmacol 72 (1) (2013) 139–146. [PubMed: 23670640]

[14]. V vere AL, Scott PJH, Clinical applications of small-molecule PET radiotracers: Current progress and future outlook, Semin. Nucl. Med 47 (5) (2017) 429–453. [PubMed: 28826519]

[15]. Damuka N, Dodda M, Sai K.K. Solingapuram, PET use in cancer diagnosis, treatment, and prognosis, in: Deep G (Ed.), Cancer Biomarkers: Methods and Protocols, Springer, US, New York, NY, 2022, pp. 23–35.

[16]. Damuka N, Sai K.K. Solingapuram, Method to development of PET radiopharmaceutical for cancer imaging, in: Deep G (Ed.), Cancer Biomarkers: Methods and Protocols, Springer, US, New York, NY, 2022, pp. 13–22.

[17]. Hou C, Hsieh C-J, Li S, Lee H, Graham TJ, Xu K, Weng C-C, Doot RK, Chu W, Chakraborty SK, Dugan LL, Mintun MA, Mach RH, Development of a positron emission tomography radiotracer for imaging elevated levels of superoxide in neuroinflammation, ACS Chemical, Neuroscience 9 (3) (2018) 578–586. [PubMed: 29099578]

[18]. Chu W, Chepetan A, Zhou D, Shoghi KI, Xu J, Dugan LL, Gropler RJ, Mintun MA, Mach RH, Development of a PET radiotracer for noninvasive imaging of the reactive oxygen species, superoxide, in vivo, Org. Biomol. Chem 12 (25) (2014) 4421–4431. [PubMed: 24847866]

[19]. Wilson AA, Sadovski O, Nobrega JN, Raymond RJ, Bambico FR, Nashed MG, Garcia A, Bloomfield PM, Houle S, Mizrahi R, Tong J, Evaluation of a novel radiotracer for positron emission tomography imaging of reactive oxygen species in the central nervous system, Nucl. Med. Biol 53 (2017) 14–20. [PubMed: 28719807]

[20]. Abe K, Takai N, Fukumoto K, Imamoto N, Tonomura M, Ito M, Kanegawa N, Sakai K, Morimoto K, Todoroki K, Inoue O, In vivo imaging of reactive oxygen species in mouse brain by using [(3)H]Hydromethidine as a potential radical trapping radiotracer, J. Cereb. Blood Flow. Metab 34 (12) (2014) 1907–1913. [PubMed: 25227606]

[21]. Pavelescu LA, On reactive oxygen species measurement in living systems, J. Med. Life 8 (Spec Issue) (2015) 38–42.

[22]. Zhang W, Cai Z, Ropchan J, Wu J, Boutagy N, Stendahl J, Chu W, Gropler R, Sinusas A, Carson R, Liu C, Huang Y, Optimized radiosynthesis of a ROS PET imaging probe for translational study, J. Nucl. Med 57 (supplement 2) (2016) 1127.

[23]. Carroll V, Michel BW, Blecha J, VanBrocklin H, Keshari K, Wilson D, Chang CJ, A boronate-caged [18F]FLT probe for hydrogen peroxide detection using positron emission tomography, J. Am. Chem. Soc 136 (42) (2014) 14742–14745. [PubMed: 25310369]

[24]. Okamura T, Okada M, Kikuchi T, Wakizaka H, Zhang M-R, A 11C-labeled 1,4-dihydroquinoline derivative as a potential PET tracer for imaging of redox status in mouse brain, J. Cereb. Blood Flow. Metab 35 (12) (2015) 1930–1936. [PubMed: 26082015]

[25]. Boutagy NE, Wu J, Cai Z, Zhang W, Booth CJ, Kyriakides TC, Pfau D, Mulnix T, Liu Z, Miller EJ, Young LH, Carson RE, Huang Y, Liu C, Sinusas AJ, In vivo reactive oxygen species detection with a novel positron emission tomography tracer, (18)F-DHMT, allows for early detection of anthracycline-induced cardiotoxicity in rodents, JACC: Basic Transl. Sci 3 (3) (2018) 378–390. [PubMed: 30062224]

[26]. Huang L, Li Z, Zhang X, Radiotracers for nuclear imaging of reactive oxygen species: advances made so far, Bioconjug Chem. 33 (5) (2022) 749–766. [PubMed: 35467335]

[27]. Sai K.K. Solingapuram, Chen X, Li Z, Zhu C, Shukla K, Forshaw TE, Wu H, Vance SA, Pathirannahel BL, Madonna M, Dewhirst MW, Tsang AW, Poole LB, Ramanujam N, King SB, Furdui CM, [(18)F]Fluoro-DCP, a first generation PET radiotracer for monitoring protein sulfenylation in vivo, Redox Biol. 49 (2022), 102218. [PubMed: 34952463]

[28]. Horemans N, Foyer CH, Asard H, Transport and action of ascorbate at the plant plasma membrane, Trends Plant Sci. 5 (6) (2000) 263–267. [PubMed: 10838618]

[29]. Yamamoto F, Sasaki S, Maeda M, Positron labeled antioxidants: Synthesis and tissue biodistribution of 6-deoxy-6-[18F]fluoro-l-ascorbic acid, International Journal of Radiation Applications and Instrumentation, Part A. Appl. Radiat. Isot 43 (5) (1992) 633–639.

[30]. Carroll VN, Truillet C, Shen B, Flavell RR, Shao X, Evans MJ, VanBrocklin HF, Scott PJH, Chin FT, Wilson DM, [(11)C]Ascorbic and [(11)C] dehydroascorbic acid, an endogenous redox pair for sensing reactive oxygen species using positron emission tomography, Chem. Commun. (Camb., Engl.) 52 (27) (2016) 4888–4890.

[31]. Sai K.K. Solingapuram, Bashetti N, Chen X, Norman S, Hines JW, Meka O, Kumar JVS, Devanathan S, Deep G, Furdui CM, Mintz A, Initial biological evaluations of 18F-KS1, a novel ascorbate derivative to image oxidative stress in cancer, EJNMMI Res. 9 (1) (2019) 43. [PubMed: 31101996]

[32]. Bansal N, Mims J, Kuremsky JG, Olex AL, Zhao W, Yin L, Wani R, Qian J, Center B, Marrs GS, Porosnicu M, Fetrow JS, Tsang AW, Furdui CM, Broad phenotypic changes associated with gain of radiation resistance in head and neck squamous cell cancer, Antioxid. Redox Signal 21 (2) (2014) 221–236. [PubMed: 24597745]

[33]. Degl'Innocenti D, Ramazzotti M, Sarchielli E, Monti D, Chevanne M, Vannelli GB, Barletta E, Oxadiazon affects the expression and activity of aldehyde dehydrogenase and acylphosphatase in human striatal precursor cells: A possible role in neurotoxicity, Toxicology 411 (2019) 110–121. [PubMed: 30391265]

[34]. Sai K.K. Solingapuram, Almaguel F, Sattiraju A, Herpai D, Debinski W, Mintz A, Radiolabeling and initial biological evaluations of [64Cu]NOTA-Pep-1L for imaging Glioblastoma (GBM), J. Nucl. Med 57 (supplement 2) (2016) 1100.

[35]. De Silva RA, Jain S, Lears KA, Chong H-S, Kang CS, Sun X, Rogers BE, Copper-64 radiolabeling and biological evaluation of bifunctional chelators for radiopharmaceutical development, Nucl. Med. Biol 39 (8) (2012) 1099–1104 [PubMed: 22743158]

[36]. Sai KKS, Huang C, Yuan L, Zhou D, Piwnica-Worms D, Garbow JR, Engelbach JA, Mach RH, Rich KM, McConathy J, (18)F-AFETP, (18)F-FET, and (18)F-FDG imaging of mouse DBT gliomas, Journal of nuclear medicine: official publication, Soc. Nucl. Med 54 (7) (2013) 1120–1126.

[37]. Damuka N, Orr M, Czoty PW, Weiner JL, Martin TJ, Nader MA, Bansode AH, Liyana Pathirannahel BS, Mintz A, Macauley SL, Craft S, Sai K. K. Solingapuram, Effect of ethanol and cocaine on [11C]MPC-6827 uptake in SH-SY5Y cells, Mol. Biol. Rep 48 (4) (2021) 3871–3876. [PubMed: 33880672]

[38]. Sai KKS, Prabhakaran J, Damuka N, Craft S, Rajagopal SA, Mintz A, Mann J, Kumar D, Synthesis and initial in vivo evaluations of [11C]WX-132-18B, a microtubule PET imaging agent, ChemistrySelect 5 (31) (2020) 9623–9625.

[39]. Reuter S, Gupta SC, Chaturvedi MM, Aggarwal BB, Oxidative stress, inflammation, and cancer: How are they linked? Free Radic. Biol. Med 49 (11) (2010) 1603–1616. [PubMed: 20840865]

[40]. Sosa V, Moliné T, Somoza R, Paciucci R, Kondoh H, Lleonart ME, Oxidative stress and cancer: An overview, Ageing Res. Rev 12 (1) (2013) 376–390. [PubMed: 23123177]

[41]. Kumar JSD, Sai K.K. Solingapuram, Prabhakaran J, Oufkir HR, Ramanathan G, Whitlow CT, Dileep H, Mintz A, Mann JJ, Radiosynthesis and in vivo evaluation of [11C]MPC-6827, the first brain penetrant microtubule PET ligand, J. Med. Chem 61 (5) (2018) 2118–2123. [PubMed: 29457976]

[42]. Sai K. Solingapuram, Huang C, Yuan L, Rich K, Mach R, McConathy J, Brain tumor imaging with the non-natural amino acid (S)-[18F]AFETP in the mouse DBT glioma model, J. Nucl. Med 52 (supplement 1) (2011) 1592.

[43]. Damuka N, Martin TJ, Bansode AH, Krizan I, Martin CW, Miller M, Whitlow CT, Nader MA, Sai K.K. Solingapuram, Initial evaluations of the microtubule-based PET radiotracer, [11C]MPC-6827 in a rodent model of cocaine abuse, Front. Med 9 (2022).

[44]. Damuka N, Orr ME, Bansode AH, Krizan I, Miller M, Lee J, Macauley SL, Whitlow CT, Mintz A, Craft S, Sai K.K. Solingapuram, Preliminary mechanistic insights of a brain-penetrant microtubule imaging PET ligand in a tau-knockout mouse model, EJNMMI Res. 12 (1) (2022) 41. [PubMed: 35881263]

[45]. Damuka N, Czoty PW, Davis AT, Nader MA, Nader SH, Craft S, Macauley SL, Galbo LK, Epperly PM, Whitlow CT, Davenport AT, Martin TJ, Daunais JB, Mintz A, Sai K.K. Solingapuram, PET imaging of [11C]MPC-6827, a microtubule-based radiotracer in non-human primate brains, Molecules 25 (10) (2020) 2289. [PubMed: 32414052]

[46]. Gazivoda T, Wittine K, Lovri I, Makuc D, Plavec J, Cetina M, Mrvoš-Sermek D, Šuman L, Kralj M, Paveli K, Mintas M, Rai -Mali S, Synthesis, structural studies, and cytostatic evaluation of 5,6-di-O-modified l-ascorbic acid derivatives, Carbohydr. Res 341 (4) (2006) 433–442. [PubMed: 16438945]

[47]. Sai KKS, Sattiraju A, Almaguel FG, Xuan A, Rideout S, Krishnaswamy RS, Zhang J, Herpai DM, Debinski W, Mintz A, Peptide-based PET imaging of the tumor restricted IL13RA2 biomarker, Oncotarget 8 (31) (2017) 50997–51007. [PubMed: 28881623]

[48]. Sai K.K. Solingapuram, Das BC, Sattiraju A, Almaguel FG, Craft S, Mintz A, Radiolabeling and initial biological evaluation of [(18)F]KBM-1 for imaging RAR-α receptors in neuroblastoma, Bioorg. Med. Chem. Lett 27 (6) (2017) 1425–1427 [PubMed: 28216044]

[49]. Sattiraju A, Sai K.K. Solingapuram, Xuan A, Pandya DN, Almaguel FG, Wadas TJ, Herpai DM, Debinski W, Mintz A, IL13RA2 targeted alpha particle therapy against glioblastomas, Oncotarget 8 (26) (2017) 42997–43007. [PubMed: 28562337]

[50]. Sergeeva O, Zhang Y, Kenyon J, Miller-Atkins G, Sergeev M, Verbus E, Iyer R, Sexton S, Kepe V, Avril N, Saunthararajah Y, Chan ER, Lee Z, Liver background uptake of [(18)F]FLT in PET imaging, Am. J. Nucl. Med Mol. Imaging 10 (5) (2020) 212–225. [PubMed: 33224617]

[51]. Ghosh KK, Padmanabhan P, Yang C-T, Mishra S, Halldin C, Gulyás B, Dealing with PETradiometabolites, EJNMMI, Research 10 (1) (2020) 109. [PubMed: 32997213]

[52]. Du J, Cullen JJ, Buettner GR, Ascorbic acid: chemistry, biology and the treatment of cancer, Biochim Biophys. Acta 1826 (2) (2012) 443–457. [PubMed: 22728050]

[53]. Schwarz SW, Oyama R, Beauvais MM, Radiochemistry and radiopharmacology, in: LIC-Nuclear Medicine and PET/CT, 11, Technology and Techniques,, 2016, p. 77.

[54]. Levine M, Padayatty SJ, Espey MG, Vitamin C: A concentration-function approach yields pharmacology and therapeutic discoveries, Adv. Nutr 2 (2) (2011) 78–88. [PubMed: 22332036]

[55]. Schlyer DJ, PET tracers and radiochemistry, Ann.-Acad. Med. Singap 33 (2) (2004) 146–154. [PubMed: 15098627]

[56]. Sai KKS, Sattiraju A, Almaguel FG, Xuan A, Rideout S, Krishnaswamy RS, Zhang J, Herpai DM, Debinski W, Mintz A, Peptide-based PET imaging of the tumor restricted IL13RA2 biomarker, Oncotarget 5 (2017).

[57]. Yamamoto Y, Nishiyama Y, Ishikawa S, Nakano J, Chang SS, Bandoh S, Kanaji N, Haba R, Kushida Y, Ohkawa M, Correlation of 18F-FLT and 18F-FDG uptake on PET with Ki-67 immunohistochemistry in non-small cell lung cancer, Eur. J. Nucl. Med. Mol. Imaging 34 (10) (2007) 1610–1616. [PubMed: 17530250]

[58]. Sai K.K. Solingapuram, Das BC, Sattiraju A, Almaguel FG, Craft S, Mintz A, Radiolabeling and initial biological evaluation of [18F]KBM-1 for imaging RAR-α receptors in neuroblastoma, Bioorg. Med. Chem. Lett 27 (6) (2017) 1425–1427. [PubMed: 28216044]

[59]. Schoenfeld JD, Sibenaller ZA, Mapuskar KA, Wagner BA, Cramer-Morales KL, Furqan M, Sandhu S, Carlisle TL, Smith MC, Abu Hejleh T, Berg DJ, Zhang J, Keech J, Parekh KR, Bhatia S, Monga V, Bodeker KL, Ahmann L, Vollstedt S, Brown H, Shanahan Kauffman EP, Schall ME, Hohl RJ, Clamon GH, Greenlee JD, Howard MA, Schultz MK, Smith BJ, Riley DP, Domann FE, Cullen JJ, Buettner GR, Buatti JM, Spitz DR, Allen BG, O(2)(·-) and H(2)O(2)-mediated disruption of Fe metabolism causes the differential susceptibility of NSCLC and GBM cancer cells to pharmacological ascorbate, Cancer Cell 31 (4) (2017) 487–500, e8. [PubMed: 28366679]

[60]. Alexander MS, Wilkes JG, Schroeder SR, Buettner GR, Wagner BA, Du J, Gibson-Corely K, Leary BR, Spitz DR, Buatti JM, Berg DJ, Bodeker KL, Vollstedt S, Brown HA, Allen BG, Cullen JJ, Pharmacological ascorbate reduces radiation-induced normal tissue toxicity and enhances tumor radiosensitization in pancreatic cancer, Cancer Res. 78 (24) (2018) 6838–6851. [PubMed: 30254147]

[61]. Robb EL, Gawel JM, Aksentijevi D, Cochemé HM, Stewart TS, Shchepinova MM, Qiang H, Prime TA, Bright TP, James AM, Shattock MJ, Senn HM, Hartley RC, Murphy MP, Selective

superoxide generation within mitochondria by the targeted redox cycler MitoParaquat, Free Radic. Biol. Med 89 (2015) 883–894. [PubMed: 26454075]

[62]. Halasi M, Wang M, Chavan TS, Gaponenko V, Hay N, Gartel AL, ROS inhibitor N-acetyl-l-cysteine antagonizes the activity of proteasome inhibitors, Biochem. J 454 (2) (2013) 201–208. [PubMed: 23772801]

[63]. Che M, Wang R, Wang H-Y, Zheng XFS, Expanding roles of superoxide dismutases in cell regulation and cancer, Drug Discov. Today 21 (1) (2016) 143–149. [PubMed: 26475962]

[64]. Ryan KA, Smith MF, Sanders MK, Ernst PB, Reactive oxygen and nitrogen species differentially regulate toll-like receptor 4-mediated activation of NF-κB and interleukin-8 expression, Infect. Immun 72 (4) (2004) 2123–2130. [PubMed: 15039334]

[65]. Costa D, Vieira A, Fernandes E, Dipyrone and aminopyrine are effective scavengers of reactive nitrogen species, Redox Rep. 11 (3) (2006) 136–142. [PubMed: 16805969]

[66]. Azad GK, Singh V, Mandal P, Singh P, Golla U, Baranwal S, Chauhan S, Tomar RS, Ebselen induces reactive oxygen species (ROS)-mediated cytotoxicity in Saccharomyces cerevisiae with inhibition of glutamate dehydrogenase being a target, FEBS Open Bio 4 (2014) 77–89.

[67]. Wagner CC, Langer O, Approaches using molecular imaging technology - use of PET in clinical microdose studies, Adv. Drug Deliv. Rev 63 (7) (2011) 539–546. [PubMed: 20887762]

[68]. Pannkuk EL, Laiakis EC, Singh VK, Fornace AJ, Lipidomic signatures of nonhuman primates with radiation-induced hematopoietic syndrome, Sci. Rep 7 (1) (2017) 9777. [PubMed: 28852188]

[69]. Sills WS, Tooze JA, Olson JD, Caudell DL, Dugan GO, Johnson BJ, Kock ND, Andrews RN, Schaaf GW, Lang RA, Cline JM, Total-Body Irradiation Is Associated With Increased Incidence of Mesenchymal Neoplasia in a Radiation Late Effects Cohort of Rhesus Macaques (Macaca mulatta), Int J. Radiat. Oncol. Biol. Phys 113 (3) (2022) 661–674. [PubMed: 35361520]

[70]. Singh VK, Olabisi AO, Nonhuman primates as models for the discovery and development of radiation countermeasures, Expert Opin. Drug Disco 12 (7) (2017) 695–709.
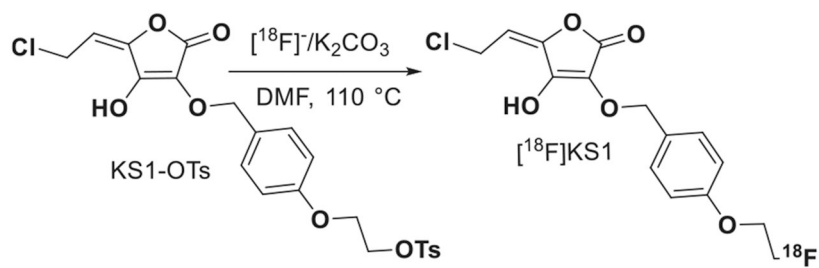
Fig. 1.
Synthetic scheme of [^{18}F]KS1 production.
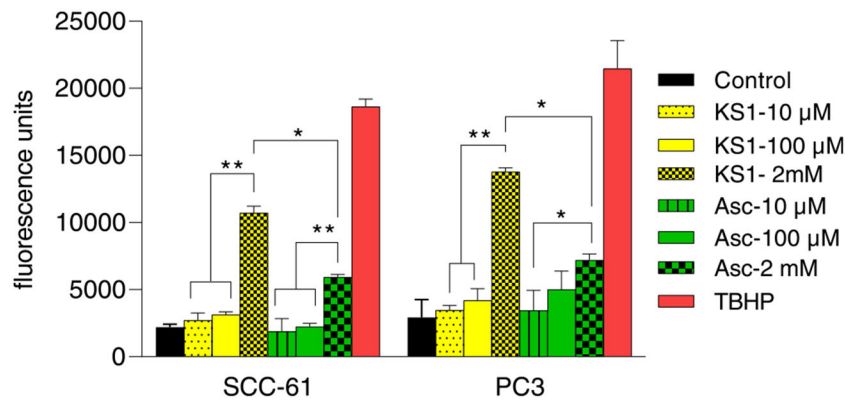
Fig. 2.
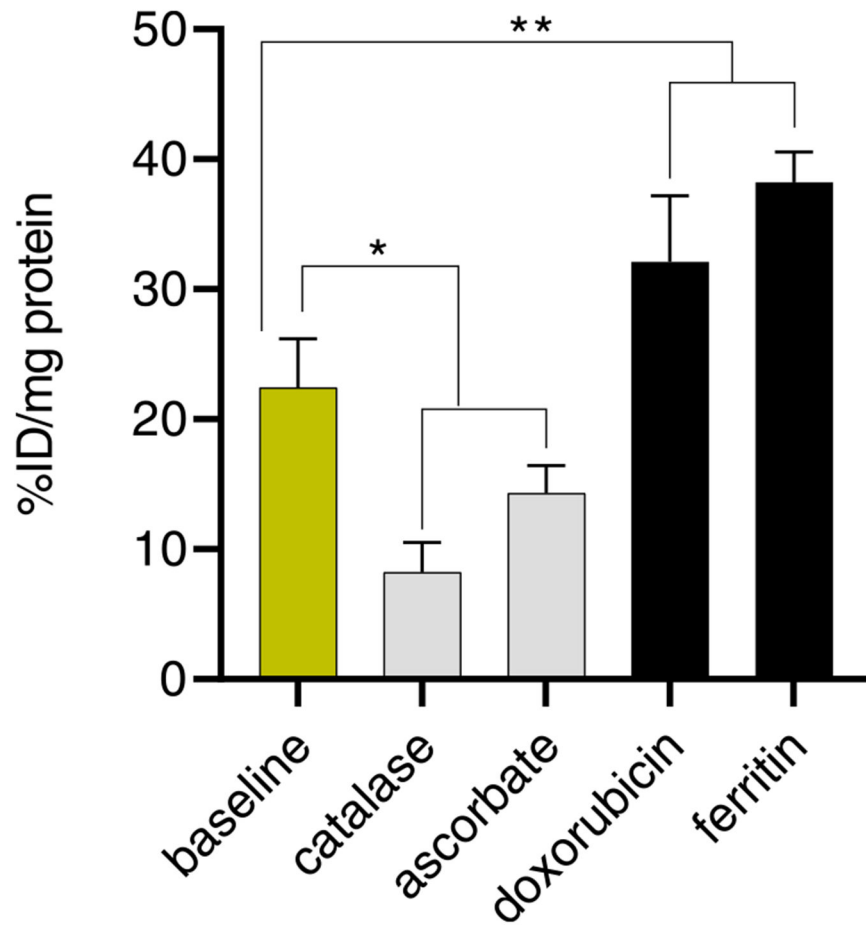DCFDA assay of KS1 and ascorbate at 10, 100 μM and 2 mM concentrations in SCC-61 and PC3 cell lines (* $p = 0.05$).
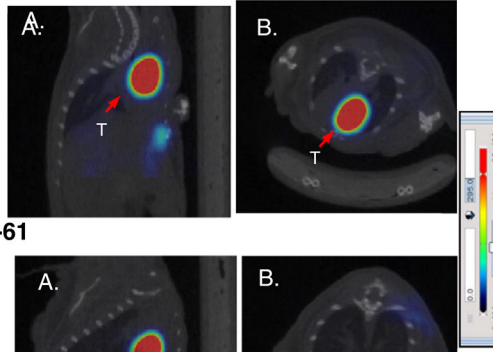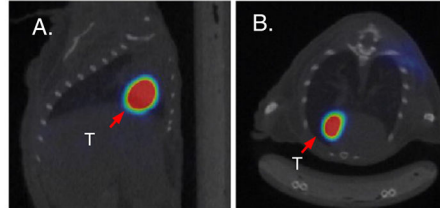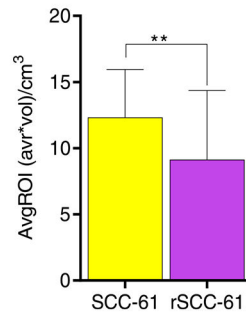
Fig. 3.
Cell uptake of [^{18}F]KS1 at baseline, ROS-blockade, and inducer conditions (n = 6/agent) in SCC-61 cells. The data were expressed as % injected dose (ID)/mg of protein present in each well, with *p = 0.04, **p = 0.005.

A. SCC-61

**B. rSCC-61**

C. tumor uptake

Fig. 4.
Representative A. sagittal and B. axial mPET/CT images of [^{18}F]KS1 in (A) SCC61 (B) rSCC-61 tumor-bearing mice and (C) their average tumor ROI-based uptake from the PET images, **$p < 0.01$. The arrow indicates the tumor (T).
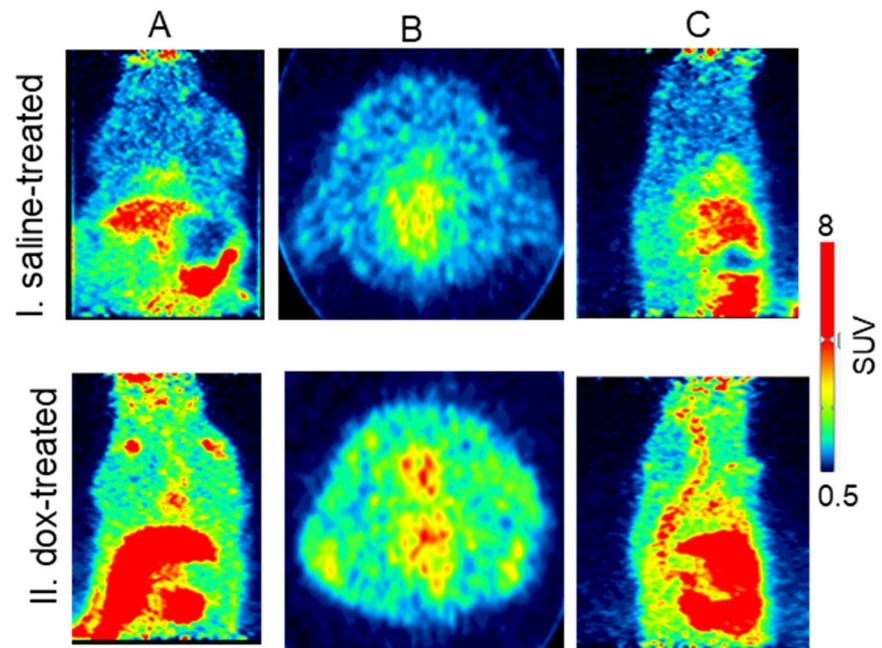
Fig. 5.
Representative A. coronal, B. axial, and C. sagittal microPET imaging of [^{18}F]KS1 in I. saline- and II. doxorubicin-treated rats.
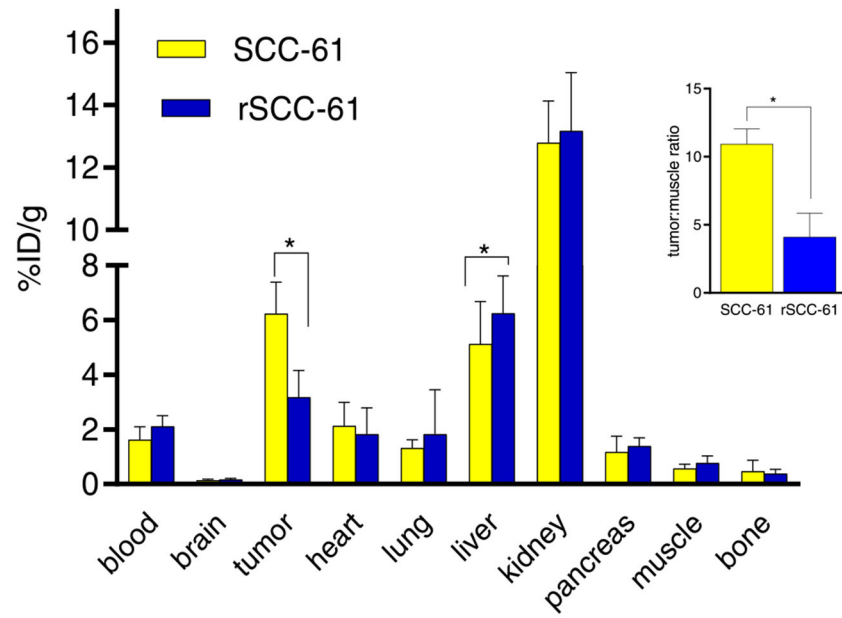
Fig. 6.
Standard biodistribution of [^{18}F]KS1 in SCC-61 and rSCC-61 tumor-bearing mice (n = 4).
Insert tumor: muscle; * p 0.05.
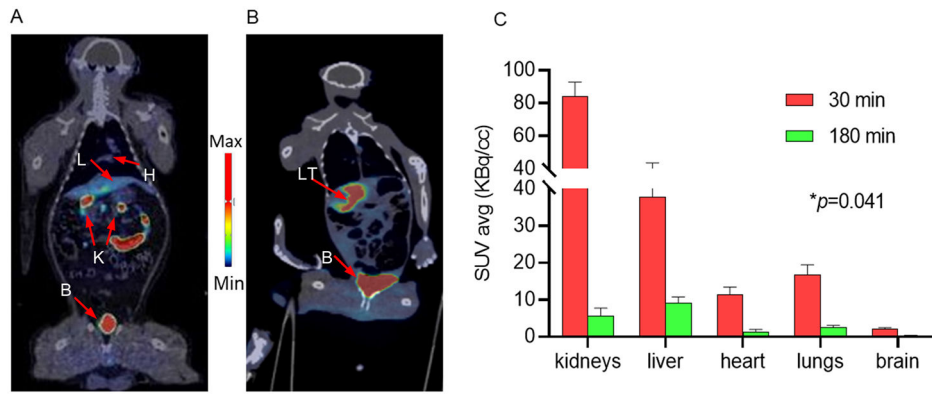
Fig. 7.
Representative coronal PET/CT images 90 min post-injection of [^{18}F]KS1 (~0.3 GBq) in a A. healthy and B. irradiated hepatic-tumor bearing rhesus monkey with their C. washout profile from 30 to 180 min from healthy rhesus monkeys (n = 4 scans). Arrows indicate L: liver, H: heart, K: kidneys, B: bladder, and LT: liver tumor.

Table 1

Biodistribution of [^{18}F]KS1 in healthy/normal mice (n = 8: 4 male and 4 female mice per time point), **p 0.001.

Organ	5 min	30 min	90 min	120 min
blood	1.361 ± 0.72	1.911 ± 0.38	1.321 ± 0.21	0.711 ± 0.071
brain	0.144 ± 0.03	0.166 ± 0.04	0.09 ± 0.01	0.11 ± 0.03
heart	1.26 ± 0.86	2.07 ± 0.96	1.74 ± 0.78	0.91 ± 0.12
lungs	1.54 ± 0.13	1.78 ± 0.63	1.02 ± 0.41	0.78 ± 0.11
liver	9.72 ± 2.55	8.24 ± 1.13	4.21 ± 0.77	2.12 ± 1.12
kidneys	14.79 ± 1.33	16.75 ± 1.86	10.21 ± 2.21	4.23 ± 0.77
pancreas	1.17 ± 0.57	1.13 ± 0.14	1.18 ± 0.51	0.78 ± 0.12
muscle	0.57 ± 0.13	0.41 ± 0.12	0.28 ± 0.11	0.18 ± 0.07
bone	0.74 ± 0.31	0.54 ± 0.30	0.22 ± 0.10	0.15 ± 0.06